Pure Appl. Geophys. 175 (2018), 1393–1404

https://doi.org/10.1007/s00024-018-1804-2

Pure and Applied Geophysics

Implications on 1 + 1 D Tsunami Runup Modeling due to Time Features of the Earthquake Source

M. Fuentes,[1] S. Riquelme,[2] J. Ruiz,[1] and J. Campos[1]

Abstract—The time characteristics of the seismic source are usually neglected in tsunami modeling, due to the difference in the time scale of both processes. Nonetheless, there are just a few analytical studies that intended to explain separately the role of the rise time and the rupture velocity. In this work, we extend an analytical 1 + 1 D solution for the shoreline motion time series, from the static case to the kinematic case, by including both rise time and rupture velocity. Our results show that the static case corresponds to a limit case of null rise time and infinite rupture velocity. Both parameters contribute in shifting the arrival time, but maximum runup may be affected by very slow ruptures and long rise time. Parametric analysis reveals that runup is strictly decreasing with the rise time while is highly amplified in a certain range of slow rupture velocities. For even lower rupture velocities, the tsunami excitation vanishes and for larger, quicker approaches to the instantaneous case.

Key words: Tsunami, seismology, runup.

1. Introduction

The study of tsunamis from analytical approaches has been treated for decades (e.g. Kajiura 1970; Carrier and Greenspan 1958; Synolakis 1987; Kânoğlu 2004; Madsen and Schaffer 2010; Fuentes et al. 2013; Fuentes 2017). However, just a few analytic studies involve explicit time characteristics of the generation process with applications to tsunamis triggered by earthquakes (Hammack 1973; Dutykh and Dias 2007; Todorovska and Trifunac 2001; Dutykh and Dias 2009). The assumption of neglecting temporal effects comes from the fact that tsunami propagation velocities are by far slower than the rupture (Kajiura 1981). Kajiura (1981) demonstrated that there was equivalence between generating a tsunami from a static seafloor displacement or from a dynamic one, because of the much lower velocity of the tsunami propagating through the source. Since then, this term has not been a subject of importance in tsunami analytical modeling.

The evidence of a variety of slow earthquakes (Ide et al. 2007) suggests at least examining and testing this hypothesis. The 2004 Sumatra–Andaman megathrust earthquake has been studied by many authors investigating the relation between earthquake and tsunami generation (Ammon et al. 2005; Lay et al. 2005; Stein and Okal 2005). These studies showed that there is a slow component on the rupture towards the north, according to Lay et al. (2005). The main excitation of the tsunami was located around 500 km from the epicenter source occurring within the first 500 s. Then, the rupture shows a slow component in the next 700–800 km and the Bengal bay brings special attention because there are large runup heights, but no high-frequency earthquake was radiated, and buildings did not show signs of damage (Lay et al. 2005). This slow component of the rupture may play an important role in the tsunami generation.

Effects of tsunami amplification along the Japanese coastline were observed by Imai et al. (2010) by modeling delayed ruptures along the Nankai trough where they caused the sub-faults to have a temporal delay resulting in the worst case scenario. This approach could be thought as the use of a variable rupture velocity. Satake et al. (2013) performed a Multi time-window inversion to resolve the time history of the slip of the 2011 Tohoku-Oki earthquake, with constant rupture velocity. They observed

[1] Department of Geophysics, Faculty of Physical and Mathematical Sciences, University of Chile, Santiago, Chile. E-mail: mauricio@dgf.uchile.cl

[2] National Seismological Center, Faculty of Physical and Mathematical Sciences, University of Chile, Santiago, Chile.

that the best delayed slip model better explained the coastal tsunami heights than the instantaneous slip model, which overestimated them. Fukutani et al. (2016) studied the uncertainties in tsunami estimations due to kinematic rupture parameters. In particular, they considered the rupture origin location and velocity along the strike direction. These kinds of studies are practical for probabilistic tsunami hazard assessments.

Regarding the analytical approach, Todorovska and Trifunac (2001) studied the problem of a hump seafloor deformation with constant rupture velocity and instantaneous source (no rise time). They found that wave amplification occurs when rupture velocity is comparable with tsunami velocity. The attributed mechanism of amplification was wave focusing. On the other hand, Dutykh and Dias (2007) modeled a seafloor deformation with a finite rise time, but simultaneously along the fault plane (instantaneous rupture). Saito and Furumura (2009) included the source duration to obtain a criterion, in terms of the fault dimensions and depth, for discriminating when a dynamic generation should be preferred over a static initial condition. Saito (2013) incorporated the rise time to evaluate the influence of dynamic tsunami generation over the ocean-bottom pressure evolution. This is useful when using in combination with ocean-bottom pressure gauges to estimate the water displacement. Nevertheless, all those studies were applied in a constant depth ocean, with the $2+1$ D linear potential theory. In this work, we trade-off one spatial dimension for bathymetry complexity. We consider a sloping beach model, which is suitable for earthquakes in subduction zones that triggers near-field tsunamis.

Geist (1998) reviewed the effects of rise time, rupture velocity, and dynamic overshooting. He used the definition of t^* as a dimensionless number from Hammack (1973). If this $t^* \ll 1$, then the static displacement is transferred immediately to the seafloor. The other extreme $t^* \gg 1$ is rare. He found that the runup decreases if the rise time increases, and the spatial variation of the rise time has almost no effects on the tsunami generation. Rise time value is between 1 and 20 s for subduction earthquakes (Geist 1998). The rupture time of the source is limited basically by two physical parameters: L and V_r, where L is the total rupture length and V_r is the rupture velocity. The source duration and the rupture time are affected depending on the rupture mode: unilateral and bilateral rupture propagation. Along-strike tsunami has a faster velocity in the ocean-ward direction because the bathymetry is deeper in that direction. Rupture modes are also important in tsunami directivity. It was demonstrated by Bouchon (1980) that, in the near field, there is a dynamic overshoot in the vertical displacement field to up-dip propagation of the rupture for an inverse fault. If the lower layer has low velocity value then the overshoot acquires an oscillatory behavior. Geist (1998) simulated this effect using the formula

$$u_z(x,t) = u_{0z}\left(1 - \cos(\omega_0 t)e^{-\frac{t}{t_R}}\right),$$

which is a ramp-like function including oscillations. Given that, the tsunami occurs in a much longer period of time than t_R.This should have a very small effect in the tsunami generation.

In this study, we will include rise time and rupture time into analytical modeling in order to study the amplification on the tsunami generation and runup.

2. Mathematical Formulation

We consider the forced linear shallow water equation in a sloping beach (Fig. 1):

$$\eta_{tt} - \alpha g(x\eta_x)_x = \eta_{0tt}, \tag{1}$$

where $\eta(x,t)$ is the water surface elevation, $\alpha =: \tan(\beta)$ is the slope of the beach, g is the gravity

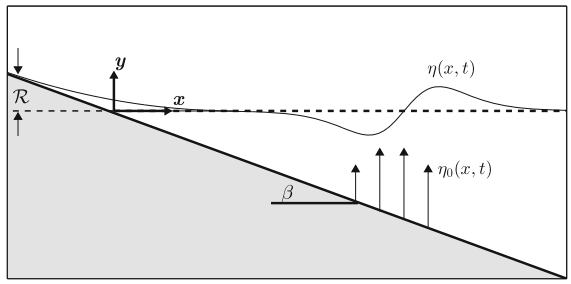

Figure 1
Sketch of the sloping beach domain and variables of the $1+1$ D model

acceleration, and $\eta_{0tt}(x,t)$ is the forcing term applied to the sea bottom.

Tuck and Hwang (1972) solved Eq. (1) by using Hankel and Laplace transforms. The solution is

$$\eta(x,t) = \int_{-\infty}^{\infty} \mathrm{J}_0(2k\sqrt{x}) \int_{-\infty}^{\infty} \mathrm{J}_0(2k\sqrt{\xi})\eta_{1tt}(\xi,t) * \sin(\sqrt{\alpha g}kt)\mathcal{H}(t)\mathrm{d}\xi\mathrm{d}k,$$

where

$$\eta_1(x,t) = \eta_0(x,t) + [\eta(x,0) + t\eta_t(x,0)]\mathcal{H}(t),$$

$\mathcal{H}(t)$ is the Heaviside step function, $J_0(\cdot)$ is the zero-order cylindrical Bessel function, and * denotes the convolution product in time.

2.1. Source Time-Dependent Solution

To model a non-instantaneous tsunami generation, we set null initial conditions, $\eta(x,0) = \eta_t(x,0) = 0$, and $\eta_0(x,t) = \zeta_0(x)T(x,t)$, where $\zeta_0(x)$ is the final shape of the seafloor deformation and $T(x,t) \in [0,1]$ is a temporal description on how $\zeta_0(x)$ is performed.T is directly related with the temporal description of the seismic source function. We define

$$T(x,t) = \left[\frac{t - t_{\mathrm{V}}}{t_{\mathrm{R}}}\mathcal{H}(t_{\mathrm{R}} + t_{\mathrm{V}} - t) + \mathcal{H}(t - t_{\mathrm{R}} - t_{\mathrm{V}})\right] \mathcal{H}(t - t_{\mathrm{V}}),$$

where t_{R} is the rise time, $t_{\mathrm{V}}(x) = \frac{|x - x_{\mathrm{R}}|}{V_{\mathrm{r}}}$ is the *rupture time* at location x for a bilateral rupture propagating with a constant velocity V_{r}, starting from an origin x_{R} (Fig. 2). For simplicity, we consider t_{R} constant.

Computing T_{tt} in the sense of the distributions, we get

$$T_{tt} = \frac{1}{t_{\mathrm{R}}}[\delta(t - t_{\mathrm{V}}) - \delta(t - t_{\mathrm{V}} - t_{\mathrm{R}})].$$

Defining

$$\mathcal{M}(\zeta,s)(t) = \frac{2}{\sqrt{\alpha g}} \int_0^{\infty} \frac{\mathcal{H}(\alpha g[t - s(\xi)]^2 - 4\xi)}{\sqrt{\alpha g[t - s(\xi)]^2 - 4\xi}} \zeta(\xi)\mathrm{d}\xi,$$

and following the same procedure as in Fuentes (2017) with each term, the approximated shoreline

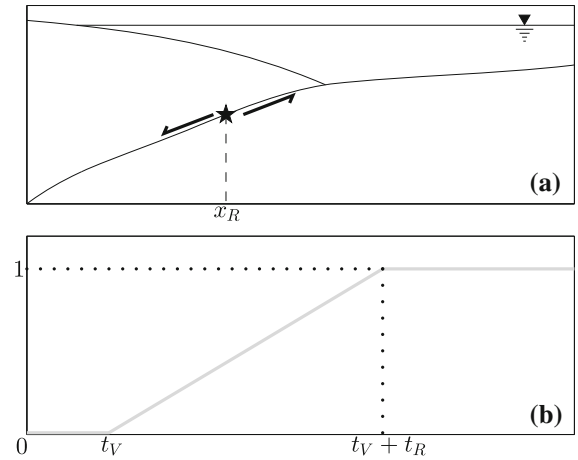

Figure 2
a Scheme of realistic setting of a subduction zone (Not to scale). The rupture origin location is denoted by x_{R}. **b** Source time function $T(x,t)$ for a given x

motion provided by the linear theory, $\eta_{\mathrm{S}}(t) =: \eta(0,t)$, can be written as

$$\eta_{\mathrm{S}}(t) = \frac{1}{t_{\mathrm{R}}}[\mathcal{M}(\zeta_0, t_{\mathrm{V}})(t) - \mathcal{M}(\zeta_0, t_{\mathrm{V}})(t - t_{\mathrm{R}})]. \quad (2)$$

From there, we can also obtain expressions for quantifying individual effects of t_{R} and V_{r}

$$\lim_{t_{\mathrm{R}} \to 0} \eta_{\mathrm{S}}(t) = \partial_t \mathcal{M}(\zeta_0, t_{\mathrm{V}})(t), \quad (3)$$

$$\lim_{V_r \to \infty} \eta_{\mathrm{S}}(t) = \frac{1}{t_{\mathrm{R}}}[\mathcal{M}(\zeta_0, 0)(t) - \mathcal{M}(\zeta_0, 0)(t - t_{\mathrm{R}})], \quad (4)$$

where Eqs. (3) and (4) are for null rise time and infinite rupture velocity, respectively.

Note that

$$\begin{aligned} \lim_{\substack{t_{\mathrm{R}} \to 0 \\ V_{\mathrm{r}} \to \infty}} \eta_{\mathrm{S}}(t) &= \lim_{\substack{V_{\mathrm{r}} \to \infty \\ t_{\mathrm{R}} \to 0}} \eta_{\mathrm{S}}(t) \\ &= \frac{2}{\sqrt{\alpha g}} \partial_t \int_0^{\infty} \frac{\mathcal{H}(\alpha g t^2 - 4\xi)}{\sqrt{\alpha g t^2 - 4\xi}} \zeta_0(\xi)\mathrm{d}\xi \\ &= \frac{1}{2}\frac{\partial}{\partial t}\left\{ t \int_0^1 \frac{\zeta_0\left(\frac{1}{4}\alpha g t^2 y\right)}{\sqrt{1 - y}} \mathrm{d}y \right\}, \end{aligned} \quad (5)$$

which is the same as the solution for the static case derived by Fuentes (2017).It is also clear to observe that

$$\lim_{V_r \to 0} \eta_S(t) = \lim_{t_R \to \infty} \eta_S(t) = 0.$$

2.2. The Seabed Deformation

As mentioned, the final shape of the initial condition is denoted by $\zeta_0(x)$. In tsunami modeling, the Okada's equations are widely used to compute the static deformation due to a finite fault in 3D (Okada 1985). It provides a solution for the problem of static deformation in an elastic half-space. Freund and Barnett (1976) solved the 2D problem of surface deformation and their solution can also handle non-uniform slip distributions.

2.2.1 Uniform Slip

We take a pure dip-slip (rake angle is 90°) fault of width W, length L, dip angle δ, slip U in a medium of Poisson ratio v.The fault is oriented parallel to the coast, so the strike angle can be fixed, in our case, to 180° due to the axis orientation chosen (Fig. 3a). In the case of a pure dip-slip fault, the slip vector reduces to $(U_1, U_2, U_3) = (0, U, 0)$.

Both studies used different coordinate system, and then they will be reoriented to our reference system.

Placing the lower corner of the fault in $\left(-\frac{L}{2}, 0, -d\right)$ and letting L tends to infinity, the Okada's solution for the seabed displacements can be reduced to the following expressions:

$$U_z(x) = u_z\left(\frac{x}{d}\right) - u_z\left(\frac{x - W\cos(\delta)}{d - W\sin(\delta)}\right), \tag{6a}$$

$$U_h(x) = u_h\left(\frac{x}{d}\right) - u_h\left(\frac{x - W\cos(\delta)}{d - W\sin(\delta)}\right). \tag{6b}$$

Originally, the retained variable should be y, but we renamed it as x to keep consistency, and it represents the variable along the half-space. u_z and u_h are the dislocations defined as

$$u_z(\bar{x}) = \frac{U}{\pi}\left[\sin(\delta)\arctan(\bar{x}) - \frac{\cos(\delta) - \bar{x}\sin(\delta)}{1 + \bar{x}^2} + (3 - 8v)\delta\sin(\delta)\right], \tag{7a}$$

$$u_h(\bar{x}) = \frac{U}{\pi}\left[\cos(\delta)\arctan(\bar{x}) - \frac{\sin(\delta) + \bar{x}\cos(\delta)}{1 + \bar{x}^2} + \sin(\delta) + \delta\cos(\delta) - 2(1 - 2v)\delta\sin(\delta)\{2\delta\tan(\delta) + 1\}\right]. \tag{7b}$$

($\bar{x}$ denotes a ratio between the horizontal distance and depth of the fault endpoint) which are the same expressions obtained by Freund and Barnett (1976) for uniform slip and corrected Madariaga (2003). It must be noted that constant terms in the previous equations were ignored by other authors. However, it is not quite important because the final displacement U_i is the difference of dislocations u_i at the endpoints

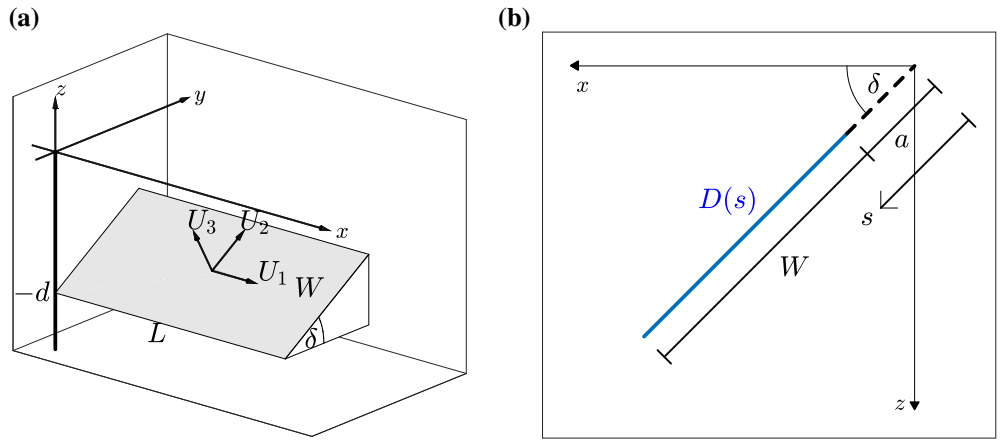

Figure 3
a Geometry and spatial orientation of the fault plane [adapted from Okada (1985)]. **b** Profile of a dip-slip fault with slip distribution $D(s)$. [adapted from Freud and Barnett (Freund and Barnett 1976)]

of the fault ($i = z, h$). Here, we will keep them for completeness.

In the worst case, the fault breaks up to the free surface of the half-space. It is well-known that a singularity is produced, but it is still possible to retain a closed form. This is obtained by letting d tends to $W\sin(\delta)^+$,

$$U_z(x) = \frac{U}{\pi}\left[\sin(\delta)\arctan\left(\frac{x}{d}\right) - \frac{d[d\cos(\delta) - x\sin(\delta)]}{x^2 + d^2} - C_1(x - W\cos(\delta))\right],$$

$$U_h(x) = \frac{U}{\pi}\left[\cos(\delta)\arctan\left(\frac{x}{d}\right) - \frac{d[x\cos(\delta) + d\sin(\delta)]}{x^2 + d^2} - C_2(x - W\cos(\delta))\right],$$

where $d = W\sin(\delta)$,

$$C_1(z) =: \frac{\pi}{2}\sin(\delta)\mathrm{sgn}(z) + \cos(\delta)\mathbf{1}_{\{0\}}(z),$$

$$C_2(z) =: \frac{\pi}{2}\cos(\delta)\mathrm{sgn}(z) + \sin(\delta)\mathbf{1}_{\{0\}}(z),$$

$\mathrm{sgn}(z)$ is the sign function and $\mathbf{1}_A(z)$ is the indicator function.

Following Tanioka and Satake (1996), the complete vertical displacement of the ocean bottom corresponds to the vertical component $U_z(x)$ plus the horizontal advection contribution. Also, we must translate the solutions to our coordinate system. Defining the trench axis location at x_0 and $x_e =: x_0 - W\cos(\delta)$,, we finally obtain

$$\zeta_0(x) = U_z(x - x_e) + \alpha U_h(x - x_e). \tag{8}$$

We can observe, when the term αU_h is neglected, that the maximum slip transformed into vertical displacement occurs in the singularity (Ward 2011); thus

$$\frac{\zeta_0(x_0)}{U} = \sin(\delta)\left(1 - \frac{\delta}{\pi}\right).$$

The optimal dip angle that maximizes the uplift is 63.76° giving 58% of slip converted into vertical displacement.

2.2.2 Non-uniform Slip

We call s to the local variable along the fault and

$$u_z(x,s) = \frac{1}{\pi}\left[\sin(\delta)\arctan\left(\frac{x - s\cos(\delta)}{s\sin(\delta)}\right) + \frac{sx\sin^2(\delta)}{x^2 - 2sx\cos(\delta) + s^2}\right], \tag{9a}$$

$$u_h(x,s) = \frac{1}{\pi}\left[\cos(\delta)\arctan\left(\frac{x - s\cos(\delta)}{s\sin(\delta)}\right) + \frac{[s - x\cos(\delta)]s\sin(\delta)}{x^2 - 2sx\cos(\delta) + s^2}\right]. \tag{9b}$$

Then, for a general slip distribution $D(s)$ and a fault of width W buried at a distance a from the origin, the final displacements are

$$U_z(x) = \int_a^{a+W} u_z(x,s)D'(s)\mathrm{d}s, \tag{10a}$$

$$U_h(x) = \int_a^{a+W} u_h(x,s)D'(s)\mathrm{d}s. \tag{10b}$$

Freund and Barnett (1976) proposed, as example, the following normalized slip distribution:

$$D'(r) = \begin{cases} \frac{12}{q^3}(q - r)r, & r < q \\ \frac{12}{(1-q)^3}(r - 1)(r - q), & r \geq q \end{cases}, \tag{11}$$

where $r = \frac{s-a}{W}$ and $q \in (0, 1)$.

In our coordinate system, $a = \frac{d}{\sin(\delta)} - W$ and the final vertical displacement is

$$\zeta_0(x) = U_z(x - x_e) + \alpha U_h(x - x_e), \tag{12}$$

with $x_e = x_0 + a\cos(\delta)$.

3. Numerical Tests

3.1. A Classical $M_w = 8.0$ Earthquake

In this section, we will set $\delta = 20°$ being a typical value in the Chilean subduction zone (Hayes et al. 2012). Once the dip angle is fixed, U and W are free to be chosen. Nonetheless, to keep realistic earthquake fault scales and to diminish the number of parameters, we use the scaling laws from Blaser et al. (2010), assuming a constant rigidity of the medium = 30GPa. Then,

$$\log(W) = -1.86 + 0.46M_w,$$

$$\log(U) = -3.15 + 0.47M_w,$$

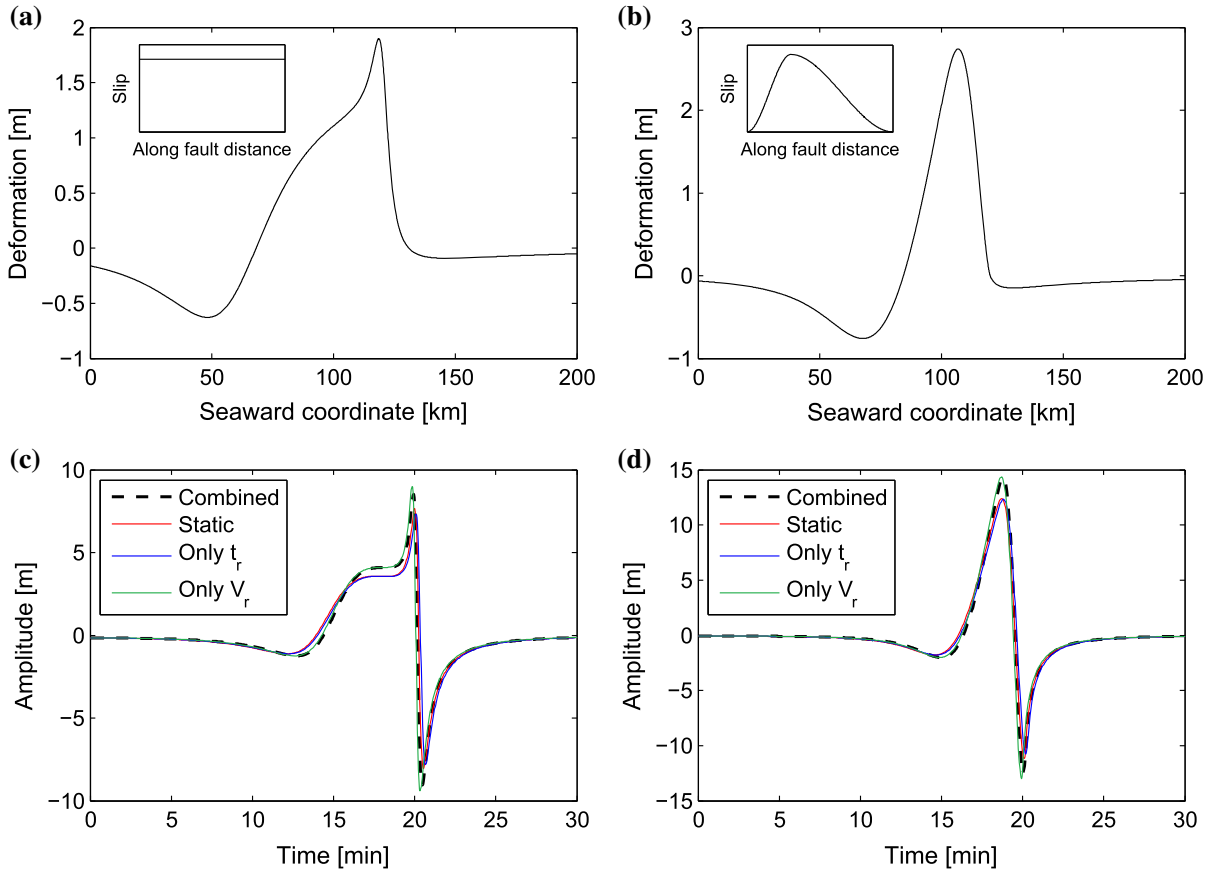

Figure 4

a Vertical displacement for a $M_w = 8.0$ earthquake (Eqs. 6a–8) computed at the sea bottom. Inner plot depicts the normalized uniform slip distribution used. **b** Vertical displacement for a $M_w = 8.0$ earthquake (Eqs. 9a, 9b, 10a, 10b, 12) computed at the sea bottom. Inner plot depicts the normalized skewed $(q = 0.3)$ slip distribution used (Eq. 11). **c** Shoreline motion induced by **a** for different cases, with $V_r = 2$ km/s, $x_R = 80$ km (asymmetric bilateral rupture) and $t_R = 15$ s (Eqs. 2–5). **d** Shoreline motion induced by **b** for different cases, with $V_r = 2$ km/s, $x_R = 80$ km (asymmetric bilateral rupture) and $t_R = 15s$ (Eqs. 2–5)

where M_w is the moment magnitude, W is in kilometers, and D is in meters. This gives $W \approx 66$ km and $D \approx 4.1$ m.

Figure 4 displays the shoreline motion due to a typical $M_w = 8.0$ earthquake for a case with uniform slip and another with non-uniform slip distribution concentrated up-dip. One can see a clear difference in the deformation profile when assuming uniform or non-uniform slip. For the values chosen in the modeling, the results show that in terms of the shoreline motion, it presents larger peak-to-peak amplitudes when considering the combined effect of t_R and V_r than in the static case. In the case of the uniform slip fault, the amplification is 11% higher when comparing a combined effect of rupture velocity and rise time with a static initial condition. The case of non-uniform slip presents a 15% of amplification. These calculations were made with values indicated in the caption of Fig. 4.

In Figs. 5 and 6, we display the complete variation of the maximum runup relative to the static case for models with rupture velocity and rise time for four modes of rupture, for two slip distributions: uniform and heterogeneous (Fig. 4). Figure 6 shows that the amplification becomes very important for low rupture velocities (of the order of the tsunami velocity). For very slow ruptures, the rise-time has little affect on the maximum runup. For larger rupture

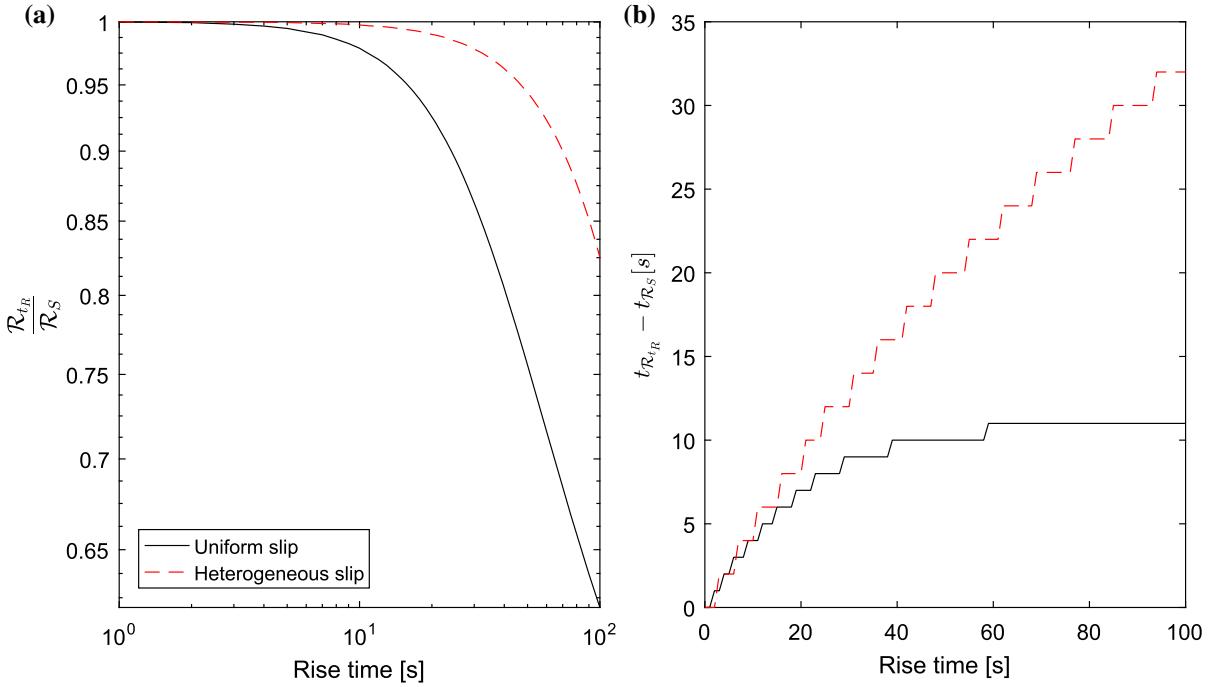

Figure 5
Effect of the rise time in the runup height and time shift for an instantaneous rupture. **a** Variation of the normalized runup (with respect to the static case) with variable rise time for homogeneous and heterogeneous slip distributions. The heterogeneous slip distribution was taken from eq. (11) with $q = 0.3$. **b** Same as **a** for the time shift relative to the peak runup time of the static case

velocities, when rise-time increases, the maximum runup tends to be in the order of the value of the static case. The complete behavior of these parameters will be examined in detail in the next section.

3.2. Parametric Analysis

There are many parameters involved in the whole problem of the tsunami runup; nonetheless, we focus on those aspects related to the temporal evolution of the source. Since the analytical solution is dependent on the initial deformation profile, we keep fixed that shape by using the same as one set in the previous subsection.

3.2.1 Rise Time

We call $\mathcal{R}_{t_R}$ the maximum runup induced by an initial condition applied with a rise time t_R, and t_1 the time where it is attained.

$$\mathcal{R}_{t_R} = \frac{1}{t_R}[\mathcal{M}(\zeta_0, t_V)(t_1) - \mathcal{M}(\zeta_0, t_V)(t_1 - t_R)].$$

Similarly, we call $\mathcal{R}_0$ the maximum runup in the case of instantaneous rise of the seafloor deformation and t_0 the time where it is attained.

$$\mathcal{R}_0 = \partial_t \mathcal{M}(\zeta_0, t_V)(t_0).$$

By virtue of the mean value theorem, there exist $\bar{t} \in (t_1 - t_R, t_1)$ such that

$$\mathcal{R}_{t_R} = \partial_t \mathcal{M}(\zeta_0, t_V)(\bar{t}).$$

Since $\mathcal{R}_0$ is the maximum of the time series,

$$\mathcal{R}_{t_R} \leq \mathcal{R}_0$$

which is true for any rise time. This result also shows that the rise time introduces a time delay in the runup. Figure (5) confirms the decreasing behavior of the ratio $\mathcal{R}_{t_R}/\mathcal{R}_0$ with increasing rise time (Fig. 5a) and also the trend that follows the time shift of the maximum runup relative to the static case (Fig. 5b). This test was performed with infinite rupture velocity,

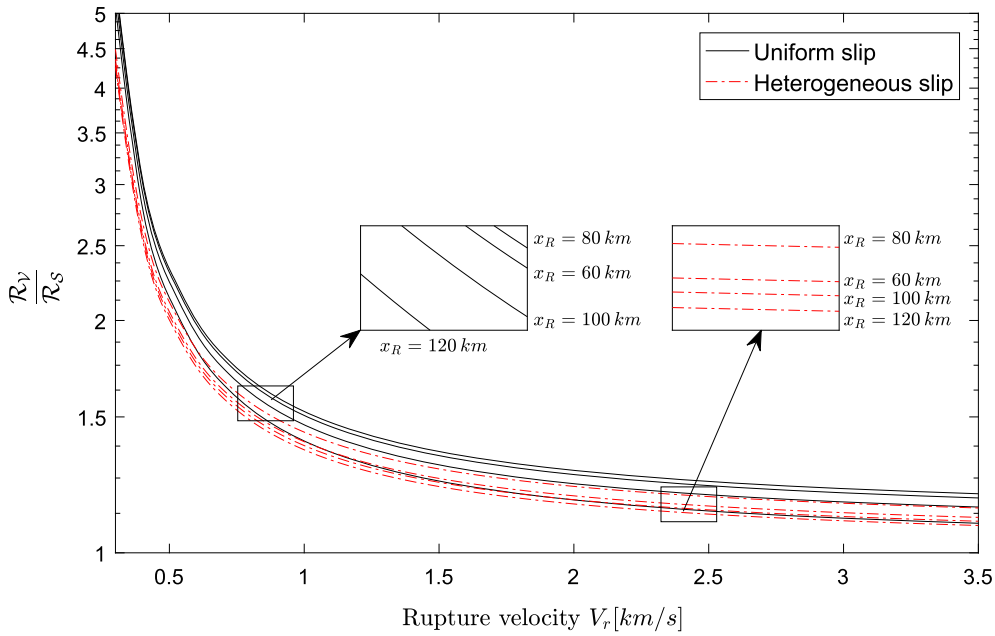

Figure 6
Amplification of the runup due to the rupture velocity considering uniform and non-uniform slip distributions. Each curve is associated with a different rupture origin location x_R. Both initial shapes were considered from subfigures (4a, b) with null rise time

which makes the origin location of the rupture x_R irrelevant.

3.2.2 *Rupture Velocity*

In this case, an analytical conclusion from the equations is more complicated to obtain. Nevertheless, we examine a wide range of rupture velocities where amplification is observed. Again, the results are compared with respect to the static case, and the rise time is set to zero in all these simulations.

Figure 6 shows the behavior of the amplification of the runup, relative to the static case, as a function of the rupture velocity. The variation with the rupture origin location reveals that the maximum amplification occurs for a bilateral rupture that initiates at the middle of the fault. Also, the amplification is greater for a rupture propagating downdip (updip origin) instead the opposite.

3.2.3 *Combined Effect of V_r and t_R*

As a summary, Figs. (7, 8) present the whole variation of the runup in terms of the rupture velocity and rise time. For instance, level curve "1" represents the isocontour where the effects of the rupture velocity and rise time are perfectly compensated. Nevertheless, as it can be deduced from the previous subsection, the worst-case scenario lies in the zone of low rupture velocities (0.3–0.5 km/s) and null rise time. Lower velocities were also tested (0.1–0.3 km/s), but numerical treatments for the integration become quite complex, even though the runup is still amplified, as founded by Todorovska and Trifunac (2001). In general, for regular earthquakes, the rupture velocity varies around 2.0–2.5 km/s and the rise time about 1–20 s (Kanamori and Brodsky 2004; Geist, 1998). This means that according to our model, the time dependency of the earthquake source is responsible for 15–20% of the amplification.

4. *Discussion and Conclusions*

Since continuous GPS and broadband seismometer observations have increased, seismologists have detected and observed several types of slow earthquakes or non-regular earthquakes such as slow slip

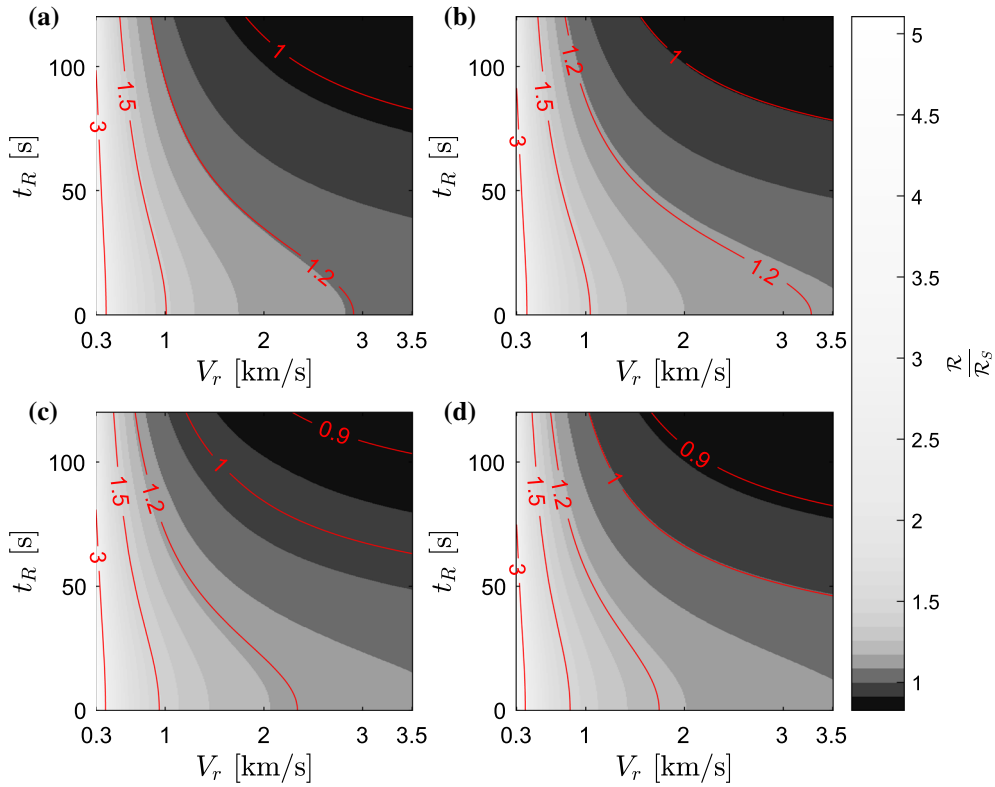

Figure 7
Color map of the maximum runup relative to the static case from Fig. 4a for four different rupture origins. **a** $x_R = 60$ km (unilateral up-dip). **b** $x_R = 80$ km (asymmetric bilateral). **c** $x_R = 100$ km (asymmetric bilateral). **d** $x_R = 120$ km (unilateral down-dip). Some level curves are displayed in red for visual guidance

events (SSE), episodic and tremors, slip earthquakes (ETS) (e.g. Miller et al. 2002; ; Beroza and Ide 2011), silent earthquakes (Kanamori and Stewart 1979), and tsunami earthquakes (Kanamori 1972) in certain zones around the world. A key question is: Do giant thrust tsunamigenic earthquakes produce slow rupture (0.1–0.5 km/s) velocities? There is no strong evidence of observations of such slow earthquake rupture velocity on tsunamigenic events in subduction zones. However, this is related to observational capabilities rather than no existence of such phenomena.

Large tsunamigenic earthquakes often produce large aftershocks immediately after the mainshock, then instruments are still reverberating for many hours. This complicates our observations of such small wave amplitudes that carry information on slow earthquake rupture velocity. Examples of this are the giant earthquakes of Valdivia 1960 and Sumatra 2004, both ruptures are very complex. The moment rate functions for both events have been subject of study (Kanamori and Cipar 1974; Lay et al. 2005; Ammon et al. 2005). These tsunamigenic earthquakes have shown slow rupture velocities; however, due to instrumental limitations, it is not well understood nor how slow they were, even the rupture area for both events were not determined until months or years after the mainshock (Barrientos and Ward 1990; Stein and Okal 2005).

For the giant 2004 Sumatra earthquake some runup observations are still not well explained, not just because of the limited resolution of the bathymetry or topography. During this event the Bay of Bengal did not experience structural damage and intensities were documented at levels I and II, suggesting the presence of a very slow rupture

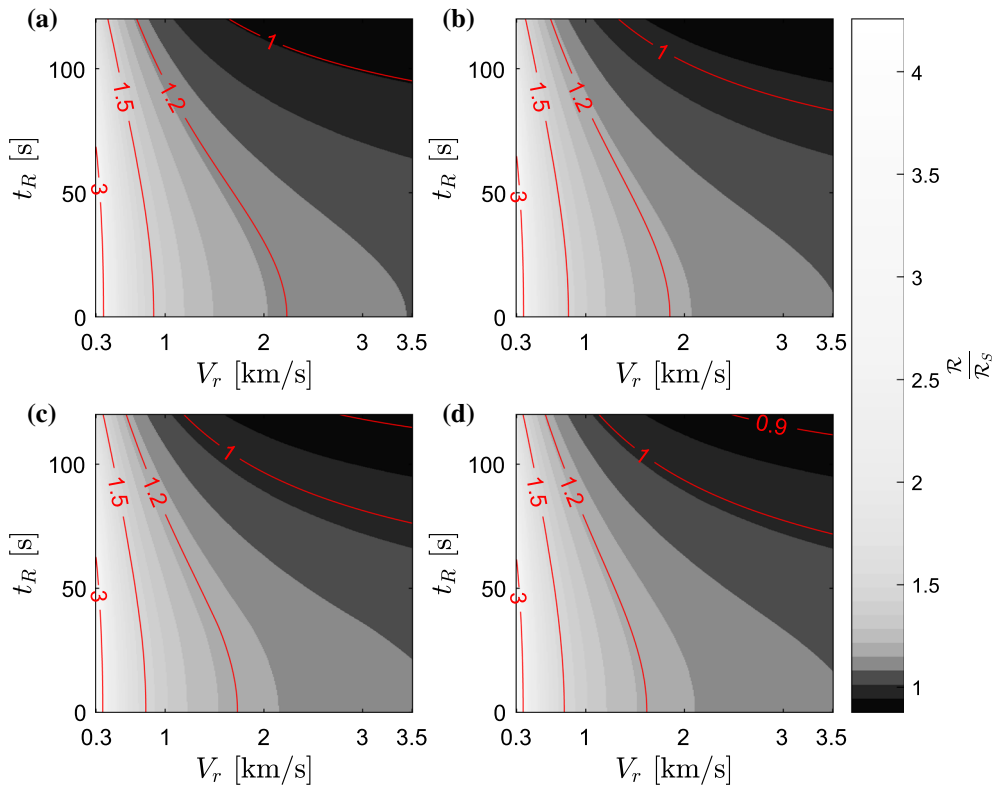

Figure 8
Color map of the maximum runup relative to the static case from Fig. 4b for four different rupture origins. **a** $x_R = 60$ km (unilateral up-dip). **b** $x_R = 80$ km (asymmetric bilateral). **c** $x_R = 100$ km (asymmetric bilateral). **d** $x_R = 120$ km (unilateral down-dip). Some level curves are displayed in red for visual guidance

component considering the inundation reached there (Lay et al. 2005). In this work, we isolate the effect of earthquake rupture velocity, rise time, and runup due to a rupture propagating along the dip direction. We computed the runup amplification due to a very slow moment rate in thrust earthquakes along the dip direction. We are aware of other amplification runup effects such as resonance in bays, shelf resonance, and edge waves. These effects are not taken into account in our analytical formulation; instead, we explore the effects on the runup due to source parameters controlling the rupture kinematic. The tsunami amplitude is larger with a slower rupture velocity (0.1–0.5 km/s) than with a regular one (2.0–2.5 km/s).

Due to the difficult equation treatment, we are still limited to obtain a solution including the source time function in the 2 + 1 D approximation. Nonetheless, with this 1 + 1 D solution we can still capture some overall features of the seismic source, and it has the advantage over previous studies that consider a sloping beach bathymetry rather than a flat ocean and the novelty of combining two temporal parameters at the same time.

We have demonstrated using a simple source model that time evolution of slip can play an important role in the tsunami modeling and its consequent runup. It cannot be neglected for some cases, especially when rupture velocities around $0.1 - 0.5$ km/s can amplify the runup up to five times compared to the static case. This suggests that the system ocean-earth resonates with the tsunami wave periods (tsunami phase velocity rounds 0.2 km/s).

Mega-large earthquakes that present slow rupture velocities, which have generated enormous tsunamis in the near-field, might be conditioned by this slow

rupture velocity component. This could be an explanation for the low earthquake intensity and the abnormal runup heights in Bengal Bay during the 2004 M_w 9.3 Sumatra earthquake. Further studies taking into account the combined effects of ruptures in the strike and dip directions are necessary to quantify accurately the amplification factors.

Acknowledgements

This work was entirely funded by the Programa de Riesgo Sísmico.

References

Ammon, C. J., Ji, C., Thio, H. K., Robinson, D., Ni, S., Hjorleifsdottir, V., et al. (2005). Rupture process of the 2004 Sumatra–Andaman earthquake. *Science, 308*(5725), 1133–1139.

Barrientos, S. E., & Ward, S. N. (1990). The 1960 Chile earthquake: inversion for slip distribution from surface deformation. *Geophysical Journal International, 103*(3), 589–598.

Beroza, G. C., & Ide, S. (2011). Slow earthquakes and nonvolcanic tremor. *Annual Review of Earth and Planetary Sciences, 39,* 271–296.

Blaser, L., Krüger, F., Ohrnberger, M., & Scherbaum, F. (2010). Scaling relations of earthquake source parameter estimates with special focus on subduction environment. *Bulletin of the Seismological Society of America, 100*(6), 2914–2926.

Bouchon, M. (1980). The motion of the ground during an earthquake: 2. The case of a dip slip fault. *Journal of Geophysical Research: Solid Earth, 85*(B1), 367–375.

Carrier, G. F., & Greenspan, H. P. (1958). Water waves of _nite amplitude on a sloping beach. *Journal of Fluid Mechanics, 4*(01), 97–109.

Dutykh, D., and Dias, F., (2007). Water waves generated by a moving bottom. In Tsunami and Nonlinear waves. In Tsunami and Nonlinear waves, 65-95. Springer Berlin Heidelberg.

Dutykh, D., & Dias, F. (2009). Tsunami generation by dynamic displacement of sea bed due to dip-slip faulting. *Mathematics and Computers in Simulation, 80*(4), 837–848.

Freund, L. B., & Barnett, D. M. (1976). A two-dimensional analysis of surface deformation due to dip-slip faulting. *Bulletin of the Seismological Society of America, 66*(3), 667–675.

Fuentes, M. (2017). Simple estimation of linear 1 + 1 D long wave run-up. *Geophysical Journal International, 209*(2), 597–605.

Fuentes, M., Ruiz, J., & Cisternas, A. (2013). A theoretical model of tsunami runup in Chile based on a simple bathymetry. *Geophysical Journal International, 196*(2), 986–995.

Fukutani, Y., Anawat, S., & Imamura, F. (2016). Uncertainty in tsunami wave heights and arrival times caused by the rupture velocity in the strike direction of large earthquakes. *Natural Hazards, 80*(3), 1749–1782.

Geist, E. L. (1998). Local tsunamis and earthquake source parameters. *Advances in Geo-physics, 39,* 117–209.

Hammack, J. L. (1973). A note on tsunamis: their generation and propagation in an ocean of uniform depth. *Journal of Fluid Mechanics, 60*(04), 769–799.

Hayes, G. P., Wald, D. J., and Johnson, R. L. (2012). Slab 1.0: A three-dimensional model of global subduction zone geometries. *Journal of Geophysical Research: Solid Earth, 117*(B1), B01302. https://doi.org/10.1029/2011JB008524.

Ide, S., Beroza, G. C., Shelly, D. R., & Uchide, T. (2007). A scaling law for slow earthquakes. *Nature, 447*(7140), 76–79.

Imai, K., Satake, K., & Furumura, T. (2010). Ampli_cation of tsunami heights by delayed rupture of great earthquakes along the Nankai trough. *Earth, Planets and Space, 62*(4), 427–432.

Kajiura, K. (1970). Tsunami source, energy and the directivity of wave radiation. *Bulletin of the Earthquake Research Institute, 48,* 835–869.

Kajiura, K. (1981). Tsunami energy in relation to parameters of the earthquake fault model. *Bulletin of the Earthquake Research Institute, 56,* 415–440.

Kanamori, H. (1972). Mechanism of tsunami earthquakes. *Physics of the Earth and Planetary Interiors, 6*(5), 346–359.

Kanamori, H., & Brodsky, E. E. (2004). The physics of earthquakes. *Reports on Progress in Physics, 67*(8), 1429.

Kanamori, H., & Cipar, J. J. (1974). Focal process of the great Chilean earthquake May 22, 1960. *Physics of the Earth and Planetary Interiors, 9*(2), 128–136.

Kanamori, H., & Stewart, G. S. (1979). A slow earthquake. *Physics of the Earth and Planetary Interiors, 18*(3), 167–175.

Kânoğlu, U. (2004). Nonlinear evolution and runup-rundown of long waves over a sloping beach. *Journal of Fluid Mechanics, 513,* 363–372.

Lay, T., Kanamori, H., Ammon, C., Nettles, M., Ward, S., Aster, R., et al. (2005). The great Sumatra–Andaman earthquake of 26 December 2004. *Science, 308*(5725), 1127–1133.

Madariaga, R. (2003). Radiation from a finite reverse fault in a half space. *Pure and Applied Geophysics, 160,* 555–577.

Madsen, P. A., & Schaffer, H. A. (2010). Analytical solutions for tsunami runup on a plane beach: single waves, N-waves and transient waves. *Journal of Fluid Mechanics, 645,* 27–57.

Miller, M. M., Melbourne, T., Johnson, D. J., & Sumner, W. Q. (2002). Periodic slow earthquakes from the Cascadia subduction zone. *Science, 295*(5564), 2423.

Okada, Y. (1985). Surface deformation due to shear and tensile faults in a half-space. *Bulletin of the Seismological Society of America, 75,* 1135–1154.

Saito, T. (2013). Dynamic tsunami generation due to sea-bottom deformation: Analytical representation based on linear potential theory. *Earth, Planets and Space, 65*(12), 1411–1423.

Saito, T., & Furumura, T. (2009). Three-dimensional tsunami generation simulation due to sea-bottom deformation and its interpretation based on the linear theory. *Geophysical Journal International, 178*(2), 877–888.

Satake, K., Fujii, Y., Harada, T., & Namegaya, Y. (2013). Time and space distribution of coseismic slip of the 2011 Tohoku earthquake as inferred from tsunami waveform data. *Bulletin of the Seismological Society of America, 103*(2B), 1473–1492.

Stein, S., & Okal, E. (2005). Speed and size of the Sumatra earthquake. *Nature, 434*(7033), 581–582.

Synolakis, C. E. (1987). The runup of solitary waves. *Journal of Fluid Mechanics, 185,* 523–545.

Tanioka, Y., & Satake, K. (1996). Tsunami generation by horizontal displacement of ocean bottom. *Geophysical Research Letters, 23*(8), 861–864.

Todorovska, M. I., & Trifunac, M. D. (2001). Generation of tsunamis by a slowly spreading uplift of the sea oor. *Soil Dynamics and Earthquake Engineering, 21*(2), 151–167.

Tuck, E. O., & Hwang, L.-S. (1972). Long wave generation on a sloping beach. *Journal of Fluid Mechanics, 51,* 449–461.

Ward, S. (2011). Tsunami. In: Gupta H.K. (eds) Encyclopedia of Solid Earth Geophysics. Encyclopedia of Earth Sciences Series. Springer, Dordrecht.

(Received June 22, 2017, revised January 20, 2018, accepted February 7, 2018, Published online February 14, 2018)